Journal of Solid State Chemistry 182 (2009) 525–531

Contents lists available at ScienceDirect

Journal of Solid State Chemistry

journal homepage: www.elsevier.com/locate/jssc

Low- and high-temperature crystal structures of TiI_3

Joachim Angelkort, Andreas Schönleber, Sander van Smaalen *

Laboratory of Crystallography, University of Bayreuth, 95440 Bayreuth, Germany

ARTICLE INFO

Article history:
Received 17 March 2008
Received in revised form
14 November 2008
Accepted 23 November 2008
Available online 3 December 2008

PACS:
61.66.Fn
61.50.Ks
64.70.kp
71.45.Lr

Keywords:
TiI_3
Phase transition
Transition metal trihalides
X-ray diffraction

ABSTRACT

Temperature-dependent, single-crystal X-ray diffraction of TiI_3 has indicated that this compound undergoes a first-order phase transition at $T_c = 323 \pm 2$ K. Accurate structural parameters are reported for the high-temperature crystal structure at $T = 326$ K (hexagonal cell, $a = 7.1416(5)$ Å, $c = 6.5102(4)$ Å, $Z = 2$, space group $P6_3/mcm$) and for the low-temperature structures at both 273 and 100 K (orthorhombic symmetry, space group $Pmnm$, $Z = 4$, lattice parameters at 273 K: $a = 12.3609(7)$ Å, $b = 7.1365(5)$ Å, $c = 6.5083(4)$ Å and at 100 K: $a = 12.2728(7)$ Å, $b = 7.0857(5)$ Å, $c = 6.4817(4)$ Å). Above T_c, TiI_3 possesses the TiI_3 structure type containing chains of equidistant metal atoms. A twofold superstructure develops below T_c, resulting in the $RuBr_3$ structure type that is characterized by a dimerization of the metal chains. The magnitude of the distortion is found to be the largest amongst the known transition metal trihalides. It thus provides an explanation for the inclination of TiI_3 towards the $RuBr_3$ structure type, despite the fact that metal–metal bonds are weaker in iodides than in chlorides or bromides.

1. Introduction

The crystal structures of transition metal halides can be characterized by a closest packed arrangement of halogen atoms with the metal atoms occupying one-third of the octahedral interstitial sites. In fluorides the metal atoms are homogeneously distributed in space, while in the other halides they are concentrated in layers or chains that are separated from each other by regions containing the empty octahedral sites [1].

The TiI_3 structure type comprises chains of equidistant metal atoms that are arranged parallel to the unique axis of a hexagonal closest packing (hcp) of iodine atoms (Figs. 1 and 2) [2]. This ordered arrangement of occupied and vacant octahedral sites possesses translational symmetry according to a threefold supercell of the hcp structure, with lattice parameters $a_h = \sqrt{3}a_{hcp}$ and $c_h = c_{hcp}$, and with the space group $P6_3/mcm$.

$RuBr_3$ crystallizes in a twofold superstructure of the TiI_3 structure type, which is characterized by the presence of dimers within the chains of metal atoms [3]. The stability of the $RuBr_3$ structure type as opposed to the TiI_3 structure type has been attributed to the presence of metal–metal bonds in the former structure [4,5]. Alternatively, the origin of the dimerization has been ascribed to the Peierls mechanism, involving quasi-one-dimensional (1D) electron bands on the chains of metal atoms [1].

$RuBr_3$ is orthorhombic with space group $Pmnm$ and lattice parameters $a_o = \sqrt{3}\,a_h$, $b_o = b_h$ and $c_o = c_h$ that define the ortho-hexagonal unit cell of the TiI_3 lattice (Fig. 1) [3]. The orthorhombic distortion of the hexagonal lattice is expressed in the diffraction by the presence of weak superlattice reflections at $(h+\frac{1}{2}, k, l)_h$ (the subscript h indicates an indexing with respect to the hexagonal lattice). Most crystals, however, are twinned with the orthorhombic structure occurring in three orientations on the hexagonal lattice [6]. While main reflections $(h, k, l)_h$ are common to the three domains, each twin domain gives rise to its own set of superlattice reflections, at $(h+\frac{1}{2}, k, l)_h$, $(h, k+\frac{1}{2}, l)_h$ and $(h-\frac{1}{2}, k+\frac{1}{2}, l)_h$, respectively.

The superlattice reflections are weak and they have been overlooked in initial studies on materials belonging to this class of compounds. It could thus be presupposed that all compounds for which the hexagonal structure has been found would actually crystallize in the $RuBr_3$ structure type. However, the question about the "true" crystal structures of transition metal halides was resolved by the notion of a phase transition between the $RuBr_3$ and TiI_3 structure types [4]. Accordingly, high-temperature (TiI_3 type) and low-temperature ($RuBr_3$ type) structures have now been reported for $RuBr_3$, $RuCl_3$ and $MoBr_3$ [7,8]. Depending

* Corresponding author. Fax: +49 921 55 3770.
E-mail address: smash@uni-bayreuth.de (S. van Smaalen).

0022-4596/$ - see front matter © 2009 Elsevier Inc. All rights reserved.
doi:10.1016/j.jssc.2008.11.028

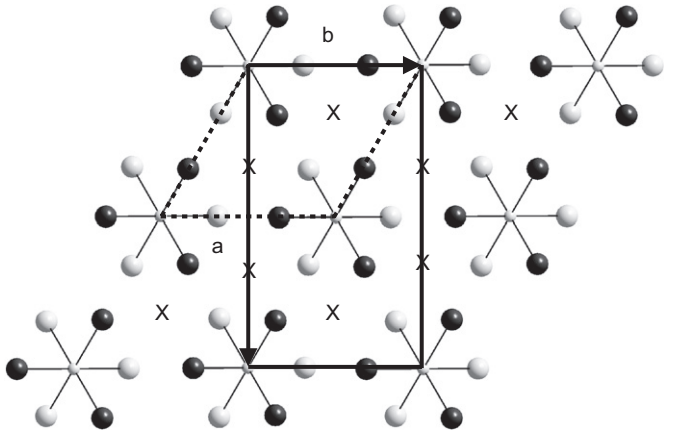

Fig. 1. Projection of the crystal structure of TiI_3 along **c**. The orthorhombic unit cell of the low-temperature structure (solid lines) is related to the hexagonal unit cell of the high-temperature structure (dotted lines) by the relations: $\mathbf{a}_o = 2\,\mathbf{a}_h + \mathbf{b}_h$, $\mathbf{b}_o = \mathbf{b}_h$ and $\mathbf{c}_o = \mathbf{c}_h$. Small spheres represent titanium atoms and big spheres iodine atoms. The *z*-coordinate of the dark iodine atoms is shifted by 0.5 from the *z*-coordinate of the light iodine atoms. Unoccupied octahedral sites are marked by crosses.

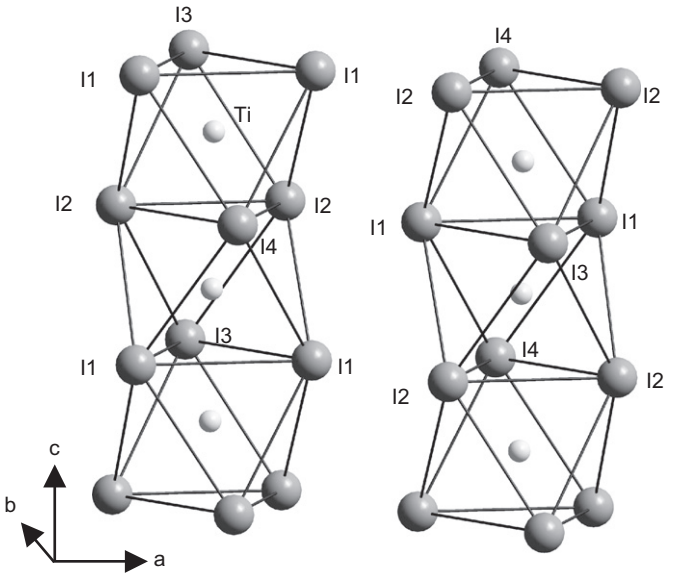

Fig. 2. Chains of face sharing TiI_3-octahedra are oriented parallel to lattice direction **c**. Atoms are labeled according to Table 6.

on the compound, transition temperatures have been found to be higher or lower than room temperature (Table 1).

The compound TiI_3 exhibits superlattice reflections in its diffraction pattern at room temperature, reflecting the $RuBr_3$ structure type [9]. The only published structure of TiI_3 is a refinement of the hexagonal substructure against the main reflections [9]. Here we report the discovery of a phase transition between the TiI_3 and $RuBr_3$ structure types at $T_c = 323 \pm 2$ K and we present accurate crystal structures of both the high-temperature and low-temperature forms. These results are analyzed in view of the mechanism of the phase transitions in transition metal halides.

2. Experimental section

TiI_3 was obtained as the result of an unsuccessful attempt to synthesize TiOI. Stoichiometric amounts of TiO_2 (Strem, 99.99%), Ti (Alfa, 99.99%) and I_2 (Alfa, 99.99%) were sealed in an evacuated quartz glass tube. This tube was placed in a temperature gradient of 923 K at the educt side and 823 K at the product side; reaction time was five days. The product consisted of pinkish-red plates, dark violet grains and black needles of several millimeters in length. The crystals were identified as TiI_2, Ti_2O_3 and TiI_3, respectively. Because TiI_3 reacts with air, the material was handled under argon and nitrogen inert atmospheres.

Two single crystals of TiI_3 were selected for X-ray diffraction experiments on an MAR345 image plate diffractometer. Crystals were mounted with the aid of vacuum grease (Krytox, DuPont) on polyamide mounts (MiTeGen [10]). The crystal temperature was regulated with a cryostream nitrogen-gas-flow cryostat, which also provided the inert atmosphere for the sample during the diffraction experiment. Diffraction data were measured by ϕ-scans of 0.5° wide. Data sets on the low-temperature phase were thus collected at temperatures of 100 and 273 K. Two runs appeared necessary for each data collection: one with an exposure time of 480 s per frame and a second one with 60 s per frame. The latter run provided the intensities of reflections that were overexposed in the first run. The software CrysAlis was used for data processing, including absorption correction [11]. Strong reflections in the data collected at both temperatures could be indexed on the basis of the hexagonal unit cell proposed by von Schnering [9] with $a_h = b_h = 7.0857(5)$ Å and $c_h = 6.4817(4)$ Å at $T = 100$ K. Much weaker reflections correspond to an apparent hexagonal $2a_h \times 2b_h \times c_h$ superlattice.

In a second experiment short runs of 10 frames each were measured temperature dependent up to 325 K (Fig. 3). Superlattice reflections were found to be present on the images up to 321 K. Some weak scattering might be present at these positions at $T = 323$ K, while the superlattice reflections were definitely absent at 325 K (Fig. 3). A complete data set was then measured at a temperature of 326 K. Data processing with CrysAlis indicated that all Bragg reflections could be indexed by the $a_h \times b_h \times c_h$ unit cell. These results are in accordance with the occurrence of a first-order phase transition in TiI_3 at a temperature of $T_c = 323 \pm 2$ K. Details on the experiments and data are given in Table 2.

3. Structure refinements

The high-temperature crystal structure of TiI_3 was refined against the data measured at $T = 326$ K. The data were averaged in Laue symmetry $6/mmm$. An excellent fit to these data was obtained in the space group $P6_3/mcm$, with the model of von Schnering [9] as start parameters. All refinements were performed with Jana2000 [12].

The low-temperature phase appeared to be orthorhombic with a primitive, orthohexagonal unit cell (Table 2). All superlattice reflections could be explained on the assumption of a threefold twinned crystal. With respect to the orthorhombic unit cell of the first domain, the superlattice reflections of the second and third domains have half-integer indices (Section 1), preventing their use in the refinement with Jana2000. Integer indices for all reflections are obtained with the hexagonal $2a_h \times 2b_h \times c_h$ superlattice (Section 2). Orthorhombic symmetry is then recovered by the non-standard centering translation $(0, \frac{1}{2}, 0)$. The latter setting was thus used for the refinement of the orthorhombic superstructure against the complete data set, taking into account the twinning. It appeared necessary to reduce the Laue symmetry of the data to $\bar{1}$, in order to allow for unequal volumes of the domains—as it proved to be the case. The shifts of the atoms towards the superstructure positions were found by the refinement using starting values of the high-temperature structure. A reasonable fit to the diffraction data was found in

Table 1
Compounds with the orthorhombic $RuBr_3$ structure type at low temperatures and the hexagonal TiI_3 structure type at high temperatures.

	$RuBr_3$ structure type				T_c (K)	TiI_3 structure type			Reference
	T (K)	a_o (Å)	b_o (Å)	c_o (Å)		T (K)	a_h (Å)	c_h (Å)	
β-$TiCl_3$	–	–	–	–	–	RT[a]	6.270	5.820	[19]
β-$TiBr_3$	–	–	–	–	–	RT[a]	6.595	6.095	[20]
TiI_3	273	12.361(1)	7.137(1)	6.508(1)	323	326	7.142(1)	6.510(1)	[*]
$RuCl_3$	170	10.576(2)	6.106(1)	5.634(1)	206	293	6.121(2)	5.655(2)	[7]
$RuBr_3$	293	11.256(2)	6.499(1)	5.873(2)	377.5	423	6.522(2)	5.885(2)	[7,8]
RuI_3	–	–	–	–	–	RT[a]	6.982	6.231	[21]
$MoBr_3$	RT	11.442(2)	6.605(1)	6.077(1)	466.1	–	–	–	[6,8]
MoI_3	–	–	–	–	–	RT[a]	7.115	6.420	[7]
$ZrCl_3$	–	–	–	–	–	RT[a]	6.383(1)	6.139(2)	[22]
$ZrBr_3$	–	–	–	–	–	RT[a]	6.728(1)	6.299(2)	[22,23]
ZrI_3	293	12.594(6)	7.292(2)	6.679(2)	–	–	–	–	[4]
HfI_3	–	–	–	–	–	RT[a]	7.225	6.59	[2]
OsI_3	–	–	–	–	–	RT[a]	6.93	6.26	[24]
NbI_3	–	–	–	–	–	RT[a]	6.61	6.82	[7]

Indicated are the temperatures at which the structures have been determined as well as the transition temperature (T_c). RT denotes room temperature.
[*] This work.
[a] Superstructure reflections were not reported, but it cannot be excluded that they were overlooked.

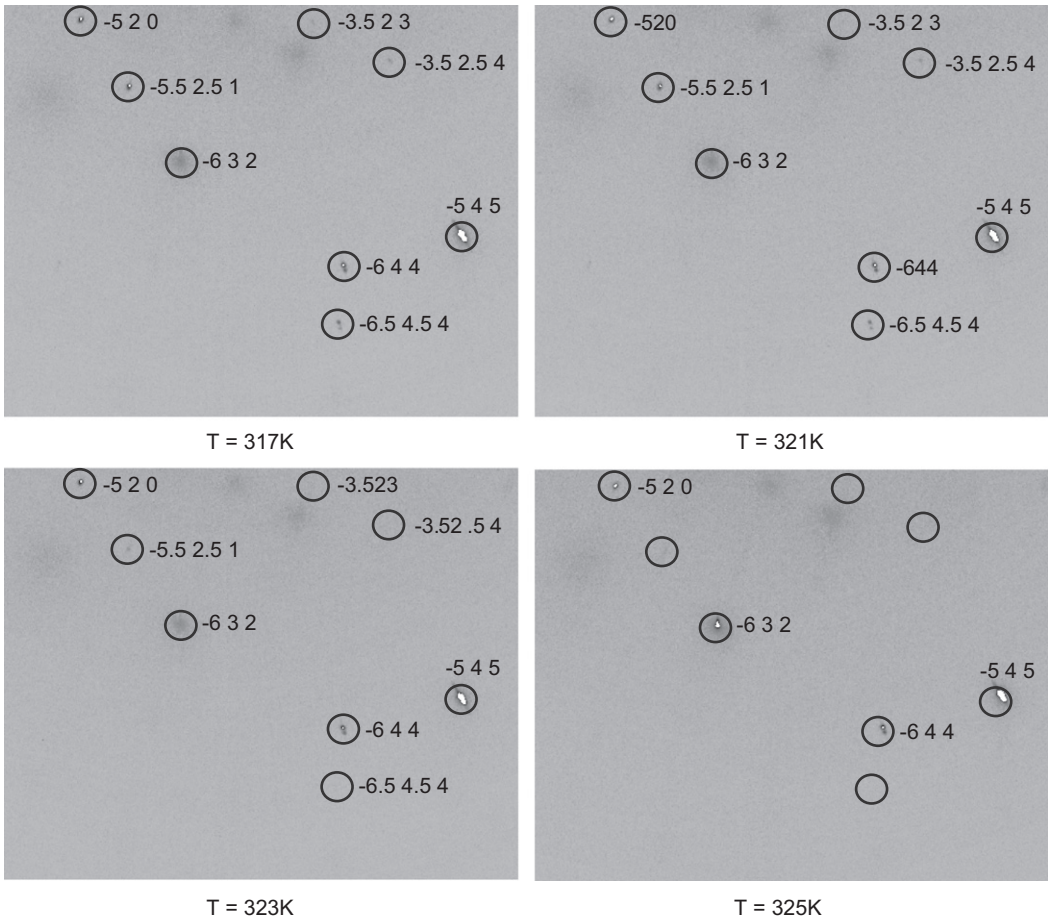

Fig. 3. Sections of MAR345-image plate frames exposed over a ϕ-range of 1.5°. The pictures show reflection spots of the same region obtained for different crystal temperatures. The indices refer to the hexagonal unit cell $\{\mathbf{a}_h, \mathbf{c}_h\}$.

space group *Pmnm* (Table 2), but *R*-values were substantially higher than for the refinement of the hexagonal structure against the high-temperature data. Atomic coordinates of the high-temperature structure are given in Table 3; Table 4 provides the atomic coordinates of the low-temperature structures with respect to the orthorhombic lattices defined in Table 2.

Motivated by the discrepancy—especially for the superlattice reflections—between calculated and observed structure factors, structure solution was tried in several orthorhombic and monoclinic space groups (Table 5). Other centrosymmetric orthorhombic space groups lead to a worse fit to the data, while an improvement of the fit could not be obtained in subgroups of

Table 2
Experimental data of the TiI_3-structure for different temperatures.

Temperature (K)	100	273	326
Formula weight (g/mol)	428.59	428.59	428.59
Crystal shape (mm^3)	$0.05 \times 0.05 \times 0.3$	$0.03 \times 0.07 \times 0.35$	$0.03 \times 0.07 \times 0.35$
Crystal system	Orthorhombic	Orthorhombic	Hexagonal
Space group	*Pmnm* (No. 59)	*Pmnm* (No. 59)	$P6_3/mcm$ (No. 193)
a (Å)	12.2728(7)	12.3609(7)	7.1416(5)
b (Å)	7.0857(5)	7.1365(5)	7.1416(5)
c (Å)	6.4817(4)	6.5083(4)	6.5102(4)
Volume ($Å^3$)	563.7	574.1	287.6
Z	4	4	2
Calculated density (g/cm^3)	5.05	4.96	4.95
Detector distance (mm)	80	80	80
Wavelength (Å)	0.71069	0.71069	0.71069
Absorption coefficient (mm^{-1})	17.78	17.45	17.43
θ_{max} (deg)	32.2	32.2	32.2
ϕ-range (deg)	180	180	150
Number of measured reflections	18 025	13 915	2636
Main	4896	3428	2636
Superlattice	13 129	10 487	–
Number of unique reflections (all)	6800	6893	201
Main	1742	1738	201
Superlattice	5058	5155	–
Number of unique reflections (obs.)	5478	4890	199
Main	1621	1585	199
Superlattice	3857	3305	–
R_{int}	0.0273	0.0258	0.0249
wR_{F^2} (observed)	0.0988	0.1150	0.0312
Main	0.0729	0.1116	0.0312
Superlattice	0.1223	0.1195	–
R_F (observed)	0.0585	0.0690	0.0137
Main	0.0361	0.0530	0.0137
Superlattice	0.1171	0.1122	–
GoF (observed)	3.33	3.90	1.52
Relative twin volumes	0.19/0.23/0.58	0.45/0.23/0.32	–
$\Delta\rho_{max}$ ($e/Å^3$)	2.22	2.20	0.45
$\Delta\rho_{min}$ ($e/Å^3$)	−2.47	−1.47	−0.49

The reflection intensities of the low-temperature measurements were averaged according to Laue symmetry $\bar{1}$. *R*-values were calculated through the expressions $R_F = (\sum \|\|F_{obs}| - |F_{cal}\|/\sum |F_{obs}|)$ and $wR_{F^2} = (\sum w(|F_{obs}| - |F_{cal}|)^2/\sum w|F_{obs}|^2)^{1/2}$ with $w = 1/((\sigma_{F_{obs}})^2 + (p\,|F_{obs}|)^2)$, in which p is the instability factor.

Table 3
Relative atomic coordinates and equivalent isotropic atomic displacement parameters ($Å^2$) for the high-temperature structure at $T = 326$ K.

	x	*y*	*z*	$\mathbf{U}_{eq}$
Ti	0	0	0	0.0243(3)
I	0.31705(4)	0	0.25	0.0246(2)

Table 4
Relative atomic coordinates and equivalent isotropic atomic displacement parameters ($Å^2$) for the low-temperature structures at $T = 100$ and 273 K.

	x	*y*	*z*	$\mathbf{U}_{eq}$
100 K				
Ti	0	−0.24646(9)	−0.22847(10)	0.0081(3)
I1	0.16325(3)	−0.40850(7)	0	0.0088(2)
I2	0.65710(4)	0.09157(8)	0	0.0088(2)
I3	0	0.07923(7)	0	0.0099(2)
I4	0.5	0.56006(8)	0	0.0093(2)
273 K				
Ti	0	−0.24678(10)	−0.22867(12)	0.0197(5)
I1	0.16255(4)	−0.40649(10)	0	0.0239(3)
I2	0.65674(5)	0.09330(10)	0	0.0241(3)
I3	0	0.07632(8)	0	0.0246(4)
I4	0.5	0.55894(10)	0	0.0230(3)

Coordinates are given with respect to the orthorhombic lattice (Table 2), with the origin of *Pmnm* at *m*2/*nm*.

Table 5
R-values of refinements of the low-temperature structure at 100 K in different space groups.

Space group	Reflection group		
	All	Main	Superlattice
$P6_3/mcm$	–	0.0391	–
Pmnm	0.0585	0.0361	0.1172
$P2_122_1$	0.0562	0.0341	0.1133
$Pmn2_1$	0.0549	0.0350	0.1066
$P2_1nm$	0.0552	0.0347	0.1085
$P12/n1$	0.0582	0.0357	0.1171
$P1n1$	0.0536	0.0347	0.1031
*P*121	0.0535	0.0337	0.1050
$P\bar{1}$	0.0550	0.0336	0.1104
Pmnn	0.1736	0.1174	0.3355
Pmcn	0.1760	0.0653	0.5086
Pmcm	0.2099	0.0848	0.5484
Pbnn	0.1676	0.0558	0.5034
Pbnm	0.1698	0.0625	0.4614
Pbcn	0.1978	0.0898	0.5369
Pbcm	0.1593	0.0542	0.4565

The value of R_F is given for all reflections, for the main reflections and for the superlattice reflections. R_F is defined as $R_F = \sum \|\|F_{obs}| - |F_{cal}\|/\sum |F_{obs}|$.

Pmnm. We therefore conclude that the low-temperature form of TiI_3 has *Pmnm* symmetry. It is noticed that the space groups $P6_3/mcm$ and *Pmnm* have previously been reported for $RuBr_3$, $RuCl_3$ and $MoBr_3$ [3,7,8], and that a similar problem of high *R*-values was reported for these compounds as well as for the

Pmnm structure of ZrI_3 [4,7,8]. A possible origin for the relatively high *R*-values might be sought in the contribution of twin boundaries—including elastic distortions of the bulk near these boundaries—to the diffracted intensities.

4. Discussion

4.1. TiI_3 and $RuBr_3$ structure types

A phase transition in TiI_3 has been found to occur at $T_c = 323 \pm 2$ K. Structure refinements establish that TiI_3 crystalizes in the TiI_3 structure type at high temperatures. Below T_c, i.e. at room temperature, TiI_3 crystalizes in the $RuBr_3$ structure type. The orthorhombic distortion follows the same pattern as it has been previously described for ZrI_3, $RuBr_3$, $RuCl_3$ and $MoBr_3$ [3,4,7,8]. Major effect is the formation of dimers along the chains of metal atoms (Fig. 2). Halogen atoms are displaced such as to keep the metal–halogen distances as equal as possible (Table 6 and [4]).

The driving force for the formation of the twofold superstructure of the TiI_3 structure type has been identified as metal–metal bonding along the chains of metal atoms [4]. At the same time the role of direct metal–metal bonding was questioned, because the transition metal triiodides have been found to crystallize more likely in the $RuBr_3$ structure type than the chlorides do, although chlorides possess shorter metal–metal distances and concomitantly stronger metal–metal bonds than the corresponding iodides. Instead, the importance was stressed of metal–metal interactions via the metal–halogen bonds [1,4].

Insight into this issue can be obtained from a consideration of the atomic valences as they can be computed from the structure models by the bond-valence method [13,14]. We have calculated bond valences for the three structures of TiI_3 reported here as well as for the high-temperature and low-temperature structures of $RuBr_3$ and $RuCl_3$ [7]. If only cation–anion interactions are taken into account the bond-valence model should lead to valence three for the metal atoms and valence one for the halogen atom. This is found to be the case for the high-temperature forms of TiI_3 and $RuBr_3$ (Table 7). For the atom pair Ru–Cl a bond-valence parameter R_0 is only available for four-valent Ru, with value $R_0(Ru^{IV}-Cl^{I}) = 2.21$ Å [14]. With this value a valence of 4.2 was obtained for Ru, which cannot be correct as is also indicated by the valence of 1.39 for Cl. We have therefore employed a value of $R_0(Ru^{III}-Cl^{I}) = 2.10$ Å, which was chosen to lead to a valence of three for Ru in the high-temperature crystal structure of $RuCl_3$ (Table 7). A difference of 0.11 Å between the bond-valence parameters of the three-valent and four-valent states of an element is untypical for the bond-valence method [13], and one could suppose that the published value [14] for $R_0(Ru^{IV}-Cl^{I})$ is actually in error.

Computed atomic valences in the $RuBr_3$ type structure are also close to three for the metal atoms in the low-temperature crystal structures of TiI_3, $RuBr_3$ and $RuCl_3$. Half of the halogen atoms appear slightly underbonded and half of them slightly overbonded, with an average valence of one (Table 7).

Cation–cation and anion–anion interactions can also be described by the bond-valence method, and bond-valence parameters for these interactions have been derived by O'Keeffe et al.

Table 6
Selected interatomic distances (Å) and bond angles (deg) at different temperatures.

	100 K	273 K	326 K
Intrachain distances			
Ti–Ti	3.520	3.532	3.255
	2.962	2.977	3.255
Ti–I1 (2×)	2.743	2.748	2.789
Ti–I2 (2×)	2.832	2.841	2.789
Ti–I3	2.742	2.744	2.789
Ti–I4	2.835	2.843	2.789
I1–I1	4.007	4.019	3.922
I1–I2 (2×)	3.944	3.949	3.965
I1–I3 (2×)	3.995	3.989	3.922
I1–I4 (2×)	3.959	3.976	3.965
I2–I2	3.856	3.875	3.922
I2–I3 (2×)	3.960	3.976	3.965
I2–I4 (2×)	3.839	3.847	3.922
Interchain distances			
I1–I1	4.089	4.129	4.174
I1–I2	4.173	4.209	4.228
I1–I2	4.173	4.211	4.228
I1–I3 (2×)	4.146	4.202	4.228
I1–I4 (2×)	4.139	4.179	4.228
I2–I2	4.170	4.205	4.174
I2–I3 (2×)	4.209	4.245	4.228
I2–I4 (2×)	4.231	4.277	4.228
I3–I4 (2×)	4.127	4.167	4.174
Bond angles			
I1–Ti–I1	93.83	93.97	89.37
I1–Ti–I2 (2×)	90.03	89.88	90.63
I1–Ti–I3 (2×)	93.48	93.14	89.37
I1–Ti–I4 (2×)	90.41	90.65	90.63
I2–Ti–I2	85.82	85.99	89.37
I2–Ti–I3 (2×)	90.54	90.75	90.63
I2–Ti–I4 (2×)	85.29	85.18	89.37
Ti–I1–Ti (2×)	65.34	65.58	71.42
Ti–I2–Ti (2×)	76.85	76.86	71.42
Ti–I3–Ti	65.38	65.68	71.42
Ti–I4–Ti	76.76	76.81	71.42

Standard uncertainties are smaller than 0.002 Å in the distances and smaller than 0.05 ° in the angles. The atom labeling is the same as in Fig. 2.

Table 7
Atomic valences of MX_3 compounds (M = Ti, Ru; X = Cl, Br, I) as computed by the bond-valence method [13,14].

	TiI_3			$RuBr_3$ [7]		$RuCl_3$ [7]	
	100 K	273 K	326 K	LT	HT	LT	HT
Valence of M	3.464	3.399	3.346	3.720	3.623	3.826	3.794
Contribution of M	0.370	0.356	0.274	0.548	0.486	0.768	0.684
Contribution of X	3.094	3.043	3.072	3.170	3.132	3.058	3.090
Valence of X_1 (2×)	−1.434	−1.411	−1.274	−1.400	−1.316	−1.286	−1.255
Contribution of M	−1.156	−1.140	−1.024	−1.124	−1.044	−1.070	−1.031
Contribution of X	−0.278	−0.271	−0.250	−0.274	−0.272	−0.214	−0.224
Valence of X_2 (2×)	−1.207	−1.170	−1.274	−1.280	−1.316	−1.192	−1.255
Contribution of M	−0.908	−0.886	−1.024	−0.990	−1.044	−0.960	−1.031
Contribution of X	−0.299	−0.284	−0.250	−0.290	−0.272	−0.232	−0.224
Valence of X_3	−1.437	−1.416	−1.274	−1.402	−1.316	−1.314	−1.255
Contribution of M	−1.159	−1.152	−1.024	−1.128	−1.044	−1.104	−1.031
Contribution of X	−0.278	−0.264	−0.250	−0.272	−0.272	−0.210	−0.224
Valence of X_4	−1.206	−1.172	−1.274	−1.276	−1.316	−1.186	−1.255
Contribution of M	−0.902	−0.882	−1.024	−0.982	−1.044	−0.952	−1.031
Contribution of X	−0.304	−0.290	−0.250	−0.292	−0.272	−0.234	−0.224
Mean valence of X	−1.320	−1.292	−1.274	−1.340	−1.316	−1.596	−1.255

Bond valences have been calculated with $b = 0.37$ Å and bond-valence parameters (from [14]): $R_0(Ti^{III}-I) = 2.54$ Å, $R_0(Ru^{III}-Br) = 2.26$ Å, $R_0(Ru^{IV}-Br) = 2.26$ Å, $R_0(Ti^{III}-Ti^{III}) = 2.52$ Å, $R_0(Ru^{III}-Ru^{III}) = 2.42$ Å, $R_0(I-I) = 2.66$ Å, $R_0(Cl-Cl) = 1.99$ Å and $R_0(Br-Br) = 2.28$ Å. And $R_0(Ru^{III}-Cl) = 2.10$ Å (see text).

Table 8
Metal–metal distances in transition metal trihalides with the $RuBr_3$ type crystal structure.

	⟨M−M⟩	M–M	M–M′	Δd
TiI_3 (273 K) [*]	3.255	2.978	3.532	0.554
$RuCl_3$ (170 K) [7]	2.817	2.633	3.001	0.368
$RuBr_3$ (293 K) [7]	2.937	2.765	3.108	0.343
ZrI_3 (RT) [4]	3.340	3.172	3.507	0.335
$MoBr_3$ (RT) [8]	3.039	2.874	3.203	0.329

Indicated are the average (⟨M−M⟩), short (M–M) and long (M−M′) distances (Å) along the metal chains as well as the difference (Δd) between the short and long distances.
[*] This work.

[15,16]. They constitute an additional contribution to the bonding of each atom. The meaning of the anion–anion bond valences is not clear to us, because they suggest that the valence of the halogen atoms would be larger than 1. For the metal atoms, however, the additional contributions to the valence can be interpreted as metal–metal bonding that brings the total valence of the metal atoms closer to the more stable valence of four of these elements (Table 7). It is thus found that the metal–metal bonding along the chains is larger in $RuCl_3$ than in $RuBr_3$ and again larger than in TiI_3, in accordance with the previous suggestion of stronger metal–metal interactions for lighter halogen atoms [4].

However, the distortion of the TiI_3 structure type towards the $RuBr_3$ structure type has a larger effect on the metal–metal bonding in the iodide than in the bromide and chloride, as it is suggested by the difference between metal atom valences in the high-temperature and low-temperature crystal structures (Table 7). The atomic distances in the $RuBr_3$ structure type indicate a stronger or at least equal dimerization in the iodides than in the bromides and chlorides (Table 8). This feature can be explained by the more flexible structures formed by the larger iodine atoms than by the smaller bromine and chlorine atoms.

4.2. The phase transition

The structural phase transitions in $RuBr_3$ and $MoBr_3$ have been characterized by temperature-dependent X-ray diffraction [7,8]. Both publications arrive at the conclusion that the phase transitions are of second order, as it is allowed by Landau theory [17]. While Hillebrecht et al. [7] state that "the metal distances change continuously in a temperature range of about 100 K around the transition temperature," Merlino et al. [8] provide a quantitative analysis of the temperature-dependent intensities of selected Bragg reflections. They have determined critical exponents (β) for the order parameter (η) in the distorted phase,

$$\eta = \left(1 - \frac{T}{T_c}\right)^{\beta} \quad (1)$$

of $\beta \approx \frac{1}{8}$. This value is only 40% of the value of $\sim\frac{1}{3}$ that is expected for the critical exponent of the order parameter of a second-order phase transition [18], and the second-order nature should be questioned.

Employing $\beta = \frac{1}{8}$ and $T_c = 323$ K in Eq. (1), the value of the order parameter in TiI_3 at $T = 273$ K is 74% of the value at 100 K. The difference in short and long metal distances, which is a measure for the magnitude of the order parameter, is nearly equal at these two temperatures and clearly at variance with a continuous change with temperature (Table 6). The other way around, the comparison of distortions at these two temperatures leads to an estimate of 0.008 for the value of the critical exponent in TiI_3. This indicates that the transition in TiI_3 is more likely to be a first-order than a second-order phase transition.

Consideration of the temperature dependence of the diffracted intensity in $MoBr_3$ [8, Fig. 9] shows that a better fit to most of the data would be possible with a value of β considerably smaller than $\frac{1}{8}$. The value $\beta \approx \frac{1}{8}$ seems to have been determined by one or two data points close to the transition temperature. These data could, however, also be explained as diffuse scattering due to critical fluctuations near the transition, and they should not have been included in the analysis of the critical exponent. We therefore propose that the transition in $MoBr_3$ is a first-order rather than a second-order phase transition. The data on $RuBr_3$ [8] encompass a much smaller range of temperatures than those on $MoBr_3$ and they seem to be less conclusive.

It is noticed that a first-order phase transition does not preclude the existence of an order parameter. The first-order character requires a discontinuity of the order parameter at T_c, while the order parameter still may continuously increase on further reduction of the temperature. Such a scenario, with different temperature dependencies below T_c, seems to explain the behaviors as observed for TiI_3, $MoBr_3$ and $RuBr_3$.

5. Conclusions

TiI_3 crystallizes in the TiI_3 structure type at high temperatures. At $T_c = 323 \pm 2$ K a structural distortion develops, resulting in the $RuBr_3$ structure type to be stable at room temperature. Similar phase transitions have been reported for $MoBr_3$, $RuBr_3$ and $RuCl_3$, whereby transition temperatures may be below or above room temperature [7,8]. These results suggest that other transition metal halides—for which either the TiI_3 or the $RuBr_3$ structure type has been reported (Table 1)—will possess such a transition too.

The high-temperature crystal structure of TiI_3 contains chains of equidistant titanium atoms. Driving force for the phase transition is metal–metal bonding through the formation of dimers along these chains, whereby the order parameter is provided by the difference between the short and long metal–metal distances. A comparison of the crystal structures of TiI_3 close to and far below T_c (Table 6), together with the analysis of scant information on this transition in other compounds (Table 1), has shown that the phase transition is most probable a first-order phase transition.

Appendix A. Supplementary data

Supplementary data associated with this article can be found in the online version at doi:10.1016/j.jssc.2008.11.028.

References

[1] J. Lin, G.J. Miller, Inorg. Chem. 32 (1993) 1476–1487.
[2] L.F. Dahl, T.-I. Chiang, P.W. Seabaugh, E.M. Larsen, Inorg. Chem. 3 (1964) 1236–1242.
[3] K. Brodersen, H.-K. Breitbach, G. Thiele, Z. Anorg. Allg. Chem. 357 (1968) 162–171.
[4] A. Lachgar, D.S. Dudis, J.D. Corbett, Inorg. Chem. 29 (1990) 2242–2246.
[5] P.K. Dorhout, J.D. Corbett, Inorg. Chem. 30 (1991) 3326–3333.
[6] D. Babel, J. Solid State Chem. 4 (1972) 410–416.
[7] H. Hillebrecht, T. Ludwig, G. Thiele, Z. Anorg. Allg. Chem. 630 (2004) 2199–2204.
[8] S. Merlino, L. Labella, F. Marchetti, S. Toscani, Chem. Mater. 16 (2004) 3895–3903.
[9] H.G. von Schnering, Naturwissenschaften 53 (1966) 359–360.
[10] R.E. Thorne, Z. Stum, J. Kmetko, K. O'Neill, R. Gillilan, J. Appl. Crystallogr. 36 (2003) 1455–1460.

[11] Software CrysAlis RED, Oxford Diffraction Ltd., Abingdon, England, 2005.
[12] V. Petricek, M. Dusek, L. Palatinus, Jana2000. The Crystallographic Computing System, Institute of Physics, Praha, Czech Republic, 2000.
[13] I.D. Brown, The Chemical Bond in Inorganic Chemistry, The Bond Valence Method, Oxford University Press, Oxford, 2002.
[14] N.E. Brese, M. O'Keeffe, Acta Crystallogr. B 47 (1991) 192–197.
[15] M. O'Keeffe, N.E. Brese, J. Am. Chem. Soc. 113 (1991) 3226–3229.
[16] M. O'Keeffe, N.E. Brese, Acta Crystallogr. B 48 (1992) 152–154.
[17] H.F. Franzen, J. Solid State Chem. 85 (1990) 173–175.
[18] P.M. Chaikin, T.C. Lubensky, Principles of Condensed Matter Physics, Cambridge University Press, Cambridge, 2000.
[19] G. Natta, P. Corrandini, G. Allegra, J. Polym. Sci. 51 (1961) 399–410.
[20] B.G. Newland, A.J. Shelton, J. Less-Common Met. 22 (1970) 369–372.
[21] H.G. von Schnering, K. Brodersen, F. Moers, H.-K. Breitbach, G. Thiele, J. Less-Common Met. 11 (1966) 288–289.
[22] E.M. Larsen, J.S. Wrazel, L.G. Hoard, Inorg. Chem. 21 (1982) 2619–2629.
[23] J. Kleppinger, J.C. Calabrese, E.M. Larsen, Inorg. Chem. 14 (1975) 3128–3130.
[24] H. Schäfer, K.-H. Huneke, C. Brendel, Z. Anorg. Allg. Chem. 383 (1971) 49–54.